SEMARAK ILMU PUBLISHING

Journal of Advanced Research in Numerical Heat Transfer

Journal homepage:
https://semarakilmu.com.my/journals/index.php/arnht/index
ISSN: 2735-0142

Transport Process of Virus Concentration from Airway to Cerebral Artery by using Computational Fluid Dynamics

Yoshiki Yanagita[1], Kaishan Feng[1], Yuko Miyamura[1,2], Adi Azriff Basri[3], Mohammad Zuber[4], Siti Rohani Mohd Yakop[5], Ahmad Fazli Abdul Aziz[6], Kamarul Arifin Ahmad[3], Masaaki Tamagawa[1,*]

[1] Graduate School of Life Science System and Engineering, Kyushu Institute of Technology, Fukuoka, Japan
[2] Department of Nursing, Faculty of Fukuoka Medical Technology, Teikyo University, Fukuoka, Japan
[3] Department of Aerospace Engineering, Faculty of Engineering, Universiti of Putra Malaysia 43400 Serdang, Selangor, Malaysia
[4] Department of Aeronautical and Automobile Engineering, Manipal Institute of Technology, Manipal Academy of Higher Education (MAHE) Manipal 576104, Karnataka, India
[5] Hospital Kuala Lumpur, Jalan Pahang, 50586 Kuala Lumpur, Malaysia
[6] Hospital Gleneagles, Kampung Berembang, 50450 Kuala Lumpur, Malaysia

ARTICLE INFO

Article history:
Received 17 September 2024
Received in revised form 18 October 2024
Accepted 16 November 2024
Available online 15 December 2024

Keywords:
Coupled Analysis; Airway; Cerebral Artery; Virus Concentration; Airway; Risk Evaluation; CFD

ABSTRACT

When a person infected with the virus releases aerosol including the virus by sneezing or talking, the virus stays in atmosphere for a long time. If other persons inhale the virus, the person maybe infected. In our previous researches, in order to decrease efficiently the risk of infection, various indoor ventilation conditions have been evaluated by analysing transport process of the virus concentration using Computational Fluid Dynamics (CFD). From them, it was found that indoor ventilation condition can be optimised by evaluating amount of the virus concentration and residence time. However, the infection process in air way and vascular when these airborne viruses from indoor air is inhaled has not been elucidated yet. In this research, a couple analysis from nasal cavity to cerebral artery via organ is tried to be applied in order to analyse the transport process of virus concentration from nasal cavity to cerebral artery. In addition, the effect of breathing waveforms and virus proliferation on the virus infection is evaluated. Regarding the methods, 3D CAD model of these three parts is created. Continuity equation, Navier-Stokes equation and transport equations of virus concentration was used as the governing equations. The transport equations in the organ are modified with the virus proliferation. Inlet boundary conditions in the nasal cavity are set up to be four types of breathing waveforms. A boundary condition between the nasal cavity and the organ is continuity of virus concentration at the contact surface. Similarly, the other boundary condition between the organ and the cerebral artery is continuity of virus concentration. As results, it was found that the virus concentration in the cerebral artery in case of sinusoidal breathing waveform with long period is the smallest. It was also found that the virus concentration in the organ and the cerebral artery in case of proliferation within the organ is higher than that has no proliferations. It is concluded that a method for minimalizing risk of virus infection can be proposed by the couple analysis.

* *Corresponding author.*
E-mail address: tama@life.kyutech.ac.jp (Masaaki Tamagawa)

https://doi.org/10.37934/arnht.28.1.5579

1. Introduction

When a person infected with the virus releases aerosol including the virus by sneezing or talking, the virus stays in atmosphere for a long time [1-5]. If other people inhale the virus, the person maybe infected [6-8]. The method of indoor ventilation for decreasing a number of people infected with the virus has been researched [9-15]. In our previous researches [9,10], in order to decrease efficiently the risk of infection, various indoor ventilation conditions have been evaluated by analyzing transport process of the virus concentration using Computational Fluid Dynamics (CFD). From them, it was found that indoor ventilation condition can be optimized by evaluating amount of the virus concentration and residence time. On the other hands, in order to associate directly the effect of the indoor ventilation with risk of infection to airway and vascular [16], unsteady concentration transport within nasal cavity has been analyzed by CFD [16-24]. The analysis is considered with virus adhered to the nasal cavity wall and pulsation due to breathing. Although this research evaluated the effects of the adhesion and the pulsation on the risk of infection, the infection process in vascular when the virus from indoor air adhered to the nasal cavity has not been elucidated yet. And also, since the virus concentration has been only compared steady flow with type of one breathing waveform, the effect of breathing waveform on the infection risk has not been sufficiently discussed.

If routes of the virus infection are assumed to be that the virus passes from the nasal cavity to the cerebral artery, it can be predicted that the routes are most likely to be between sphenoid sinus and internal carotid artery. Because the distance between the nasal cavity and the cerebral artery is very close [25]. It is important to be tried to make an analysis of the infection process as shown above and to investigate interrelationship of virus concentration between the airway and vascular. In addition, it is necessary to assume to be that the virus proliferates within the tissues during incubation time [26], and the proliferated virus reaches the cerebral artery.

In this research, a couple analysis from nasal cavity to cerebral artery via organ is tried to be applied in order to analyze the transport process of them (Figure 1). In addition, the effect of breathing waveforms and virus proliferation on the virus infection is evaluated. The breathing waveforms in the nasal cavity is four types: steady flow for standards, simulated waveform combined multiple sine function, two types of the simple sine functions changed periods of breathing. The breathing waveforms which the virus concentration in the cerebral artery is the smallest, was proposed. And also, the effect of the virus proliferations was evaluated by the ratio of virus concentration in the nasal cavity to the cerebral artery.

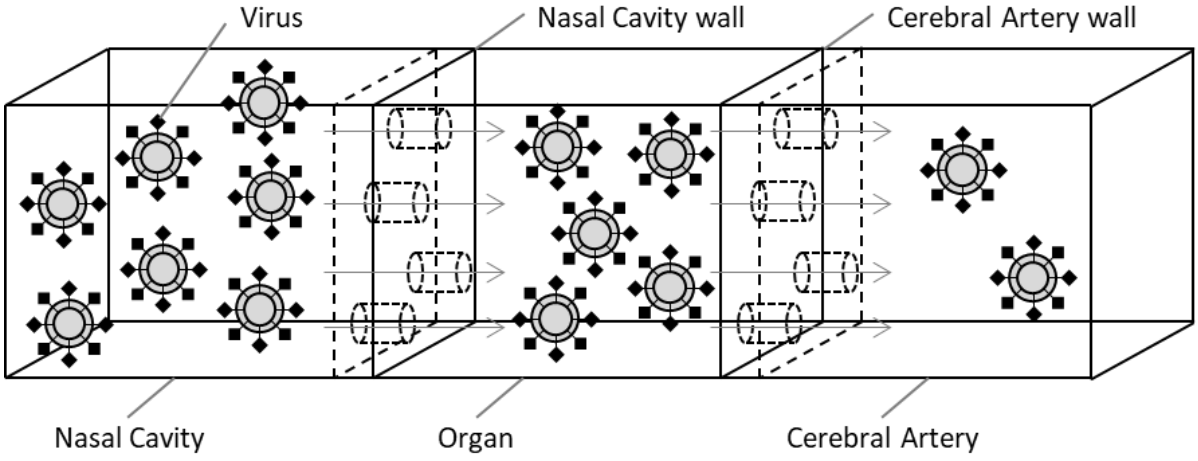

Fig. 1. Schematic diagram of a couple analysis from nasal cavity to cerebral artery via organ

2. Methodology

2.1 Objective Geometries

In order to apply a coupled analysis from the nasal cavity to the cerebral artery, 3D CAD model of these three parts are created: nasal cavity, organ and cerebral artery. In second steps, the transport process of virus concentration from the nasal cavity to the cerebral artery via organ is analyzed by CFD. Then, the effect of breathing waveform and the virus proliferation on the risk of infection is investigated.

The models of the nasal cavity and the cerebral artery are created from medical images [27,28], and the model of the organ is made by cutting out the created two models from the simple rectangular geometry. Figure 2 shows the models of the nasal cavity, the organ, and the cerebral artery. Figure 2(a) shows the nasal cavity, Figure 2(b) shows the organ, and Figure 2(c) shows the cerebral artery. These models are created from medical image of patient 42 age. Figure 3 shows an analytical model combined these models shown in Figure 2. A boundary condition between the nasal cavity and the organ is continuity of virus concentration at the contact surface. Similarly, the other boundary condition between the organ and the cerebral artery is continuity of virus concentration.

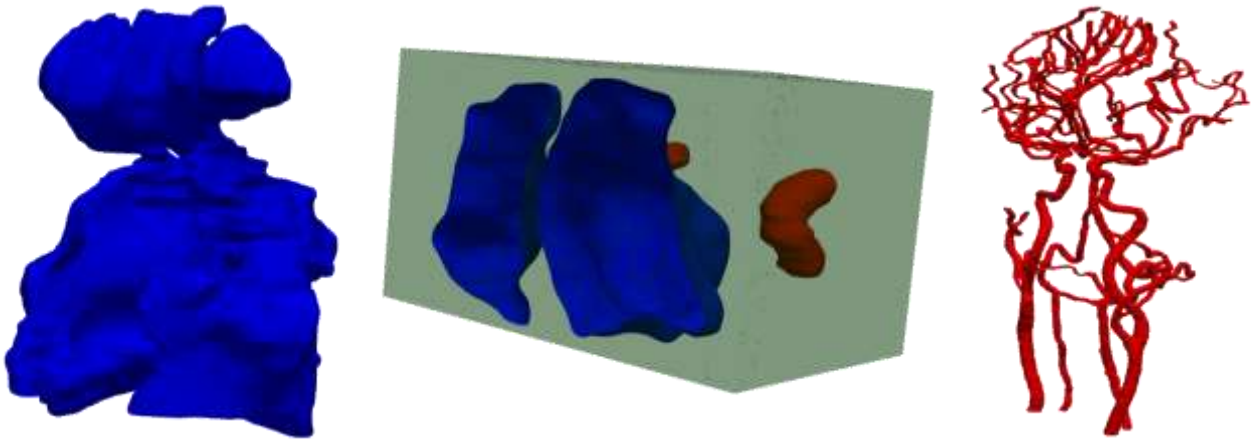

(a) (b) (c)

Fig. 2. Objective geometries of (a) nasal cavity, (b) organ, and (c) cerebral artery

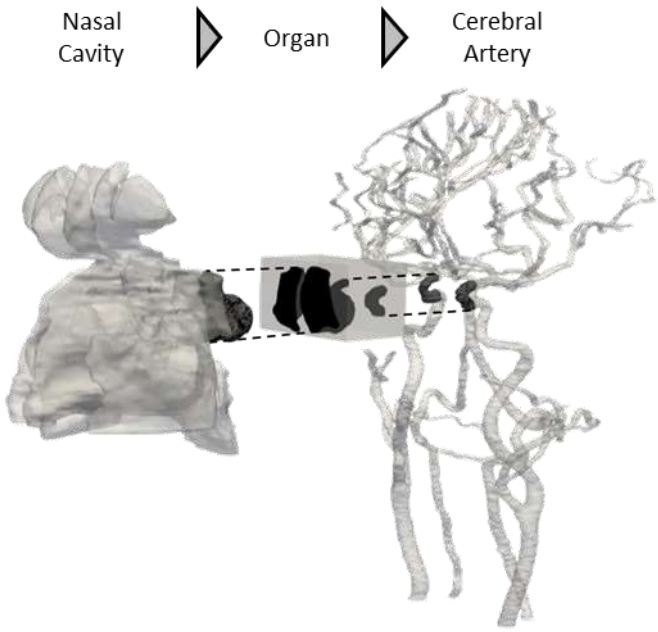

Fig. 3. Coupled model of nasal cavity, organ and cerebral artery

2.2 Governing Equations and Boundary Conditions
2.2.1 Nasal cavity

In this paper, the transport process of virus concentration from the nasal cavity to the cerebral artery via organ is analyzed by CFD. Generally, the flow in nasal cavity is the complicated flow mixed laminar and turbulent flow, and the flow is controlled by pulsating due to breathing. Regarding the flow in the nasal cavity, it is assumed to be turbulent incompressible unsteady flow. The governing equations is Continuity equation and Navier-Stokes equation,

$$\boldsymbol{\nabla} \cdot \boldsymbol{u_{nas}} = 0 \tag{1}$$

$$\frac{\partial \boldsymbol{u_{nas}}}{\partial t} + \boldsymbol{\nabla} \cdot (\boldsymbol{u_{nas}} \boldsymbol{u_{nas}}) = -\frac{1}{\rho_{nas}} \boldsymbol{\nabla} p_{nas} + \left(\nu_{nas} + \nu_{t,nas}\right) \boldsymbol{\nabla}^2 \boldsymbol{u_{nas}} \tag{2}$$

where $\boldsymbol{u_{nas}}$ is velocity, ρ_{nas} is density, p_{nas} is pressure, ν_{nas} is kinematic viscosity, $\nu_{t,nas}$ is coefficient of turbulence (= $C_\mu \rho_{nas} k^2/\varepsilon$). Also, the turbulence model is k- εmodel, and the coefficient of turbulence in the Eq. (2) is calculated by using k and ε. The governing equations for getting k and ε are following equations,

$$\frac{\partial k}{\partial t} + \boldsymbol{u_{nas}} \boldsymbol{\nabla} k = -\boldsymbol{u_{nas}} \boldsymbol{u_{nas}} \boldsymbol{\nabla} \boldsymbol{u_{nas}} + \boldsymbol{\nabla} \left\{ \left(\frac{\nu_{t,nas}}{\sigma_k} + \nu \right) \boldsymbol{\nabla} k \right\} \tag{3}$$

$$\frac{\partial \varepsilon}{\partial t} + \boldsymbol{u_{nas}} \boldsymbol{\nabla} \varepsilon = \left(-C_{\varepsilon 1} \boldsymbol{u_{nas}} \boldsymbol{u_{nas}} \boldsymbol{\nabla} \boldsymbol{u_{nas}} - C_{\varepsilon 2} \varepsilon\right) \frac{\varepsilon}{k} + \boldsymbol{\nabla} \left\{ \left(\frac{\nu_{t,nas}}{\sigma_\varepsilon} + \nu \right) \boldsymbol{\nabla} \varepsilon \right\} \tag{4}$$

where $C\mu$(= 0.09), σ_k (= 1.0), $C_{\varepsilon 1}$ (= 1.44), $C_{\varepsilon 2}$ (= 1.92), σ_ε (= 1.3) are model coefficient. The virus concentration in the nasal cavity is defined by following equation.

$$\frac{\partial c_{nas}}{\partial t} + \boldsymbol{\nabla} \cdot (\boldsymbol{u_{nas}} c_{nas}) - \left(D_{m,nas} + D_t\right) \boldsymbol{\nabla}^2 c_{nas} = 0 \tag{5}$$

where c_{nas} is virus concentration, $D_{m,nas}$ is molecular diffusion coefficient [16], D_t is turbulence diffusion coefficient (= $\nu_{t,nas}/Sc_t$), Sc_t is turbulence Schmidt number (= 1). As Viral aerosol diameter assumed to be 1μm, the molecular diffusion coefficient was defined by using Stokes-Einstein equation. The concentration of virus aerosol is defined 4.98×10^{-11} mol/m^3. This value is that a mass of virus included in droplet measured in previous research is divided by the volume gotten from the assumed aerosol diameter (=1 μm)[29,30].

The boundary condition in the nasal cavity is explained. Figure 4 shows the location of boundary condition for the nasal cavity at inlet, outlet and wall. Inlet boundary condition is assumed to be that the pressure gradient is 0, the velocity is defined types of four breathing waveforms, and the virus concentration gradient is 0. Outlet boundary condition is assumed to be that the pressure is 0 Pa, the velocity gradient is 0, and the virus concentration gradient is 0. Wall boundary condition is assumed that the pressure gradient is 0, the velocity is 0 m/s, and the virus concentration is condition for virus attachment to the wall. The condition is defined by following equations,

$$\frac{\partial c_{nas}}{\partial n} = -\frac{J}{D_{m,nas}} \tag{6}$$

$$J = k_{coff} c_{nas} \tag{7}$$

where J is virus concentration flux, k_{coff} is virus attachment coefficient. The virus concentration flux is calculated by Eq. (7). This equation can be gotten by applying newton's cooling law to the condition of virus attachment. Wall boundary conditions for virus adhesion can be set up by substituting the calculated virus concentration flux into Eq. (6). The virus attachment coefficient is defined by previous research [31].

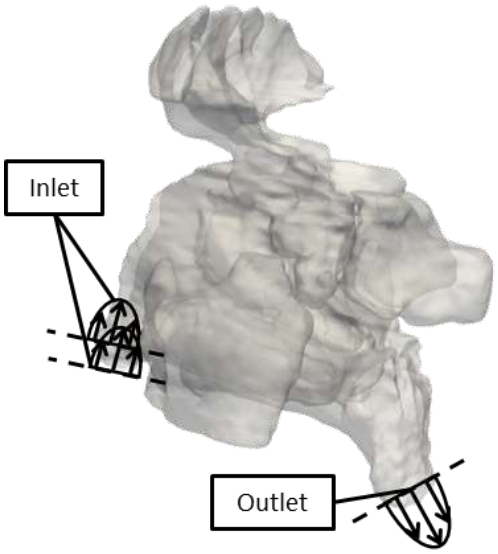

Fig. 4. Location of the boundary conditions for the nasal cavity at Inlet, Outlet and Wall

2.2.2 Organ

The virus concentration in the organ is defined by the virus concentration transport equation included time-derivative term and diffusion term,

$$\frac{\partial c_{org}}{\partial t} - D_{m,org}\boldsymbol{\nabla}^2 c_{org} = 0 \tag{8}$$

where c_{org} is virus concentration, $D_{m,org}$ is molecular diffusion coefficient. The virus concentration transport equation considered with virus proliferation is defined by modifying Eq. (8) as shown in the following equation.

$$\frac{\partial [f(t)c_{org}]}{\partial t} - D_{m,org}\boldsymbol{\nabla}^2 \left[f(t)c_{org}\right] = 0$$
$$\frac{\partial c_{org}}{\partial t} - D_{m,org}\boldsymbol{\nabla}^2 c_{org} = -\alpha c_{org} \tag{9}$$

The boundary condition in the organ is explained. Figure 5 shows the location of boundary condition for the organ at inlet, outlet and wall. Inlet boundary condition is assumed to be that the virus concentration is continuity of virus concentration at the contact surface. The boundary condition of the virus concentration is defined by following equations,

$$c_{org} = T_{org} c_{nas} \tag{10}$$

where T_{org} is the transmission rate of virus concentration between the nasal cavity and the organ. Considering the transmittance rate from a biological perspective, ion channels open and close depending on the ion state near nasal cavity wall. The ion channels assumed a porous layer. The transmittance rate is defined the rate at which viruses pass through the nasal cavity wall assumed to be the porous layer. Outlet and wall boundary condition is assumed to be that the virus concentration gradient is 0.

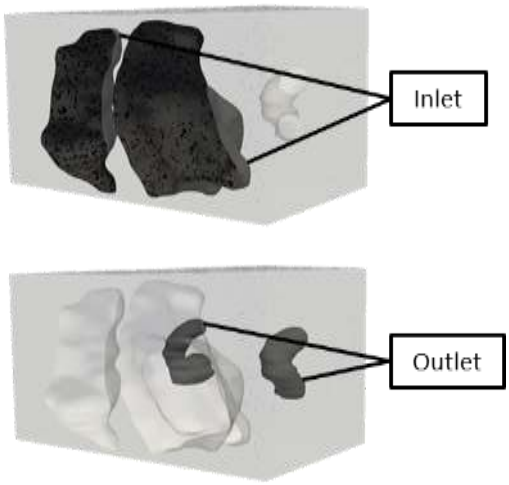

Fig. 5. Location of the boundary conditions for the organ at Inlet, Outlet and Wall

2.2.3 Cerebral artery

Generally, the flow in the cerebral artery is laminar flow, and pulsatile flow is with heart pulsation. Regarding the flow in the cerebral artery, it is assumed to be laminar incompressible unsteady flow. The governing equations is Continuity equation and Navier-Stokes equation,

$$\boldsymbol{\nabla} \cdot \boldsymbol{u_{art}} = 0 \tag{11}$$

$$\frac{\partial \boldsymbol{u_{art}}}{\partial t} + \boldsymbol{\nabla} \cdot (\boldsymbol{u_{art}} \boldsymbol{u_{art}}) = -\frac{1}{\rho_{art}} \boldsymbol{\nabla} p_{art} + \nu_{art} \boldsymbol{\nabla}^2 \boldsymbol{u_{art}} \tag{12}$$

where $\boldsymbol{u_{art}}$ is velocity, ρ_{art} is density, p_{art} is pressure, ν_{art} is kinematic viscosity.

The virus concentration in the cerebral artery is defined by following virus concentration transport equation,

$$\frac{\partial c_{art}}{\partial t} + \boldsymbol{\nabla} \cdot (\boldsymbol{u_{art}} c_{art}) - D_{m,art} \boldsymbol{\nabla}^2 c_{art} = 0 \tag{13}$$

where c_{art} is virus concentration, $D_{m,art}$ is molecular diffusion coefficient.

The boundary condition in the cerebral is explained. Figure 6 shows the location of boundary condition for the cerebral artery at inlet, outlet and wall. Inlet boundary surfaces are four: LCA, RCA, LVA and RVA. Inlet boundary condition is assumed to be that the pressure gradient is 0, the velocity is set up based on the velocity waveform of the carotid artery [32]. These waveforms are defined by following equation,

$$Q_{art}(t) = A_{art} \beta \left\{ a_0 + \sum_{i=1}^{4} a_i \, cos\left(\frac{2\pi i}{T} t\right) + b_i \, sin\left(\frac{2\pi i}{T} t\right) \right\} \tag{14}$$

$$\boldsymbol{u_{art}}(r, t) = \frac{Q_{art}(t)}{A_{art}} \left(1 - \left(\frac{r}{R}\right)^2\right) \tag{15}$$

where A_{art} is area at Inlet in the cerebral artery, β is flow rate adjustment coefficient, a_i and b_i are model coefficient. Table 1 shows the model coefficient in the Eq. (14). The amplitude of the velocity waveform was adjusted so that the averaged velocity of LCA and RCA was 0.26 m/s. In addition, the amplitude of the velocity waveform was adjusted by some method so that the average velocity of LVA and RVA was 0.255 m/s. Inlet boundary condition is assumed to be that the virus concentration gradient is 0. Outlet boundary condition is assumed to be that the pressure is 0 Pa, the velocity gradient is 0, and virus concentration gradient is 0. Wall boundary condition is assumed that the pressure gradient is 0, the velocity is 0m/s, and the virus concentration is continuity of virus concentration at the contact surface. The boundary condition of the virus concentration is defined by following equations,

$$c_{art} = T_{art} c_{org} \tag{16}$$

where T_{art} is the transmission rate of virus concentration between the organ and the cerebral artery. In addition, wall boundary condition in the region where the organ and the cerebral artery are not contact is that the virus concentration gradient is 0.

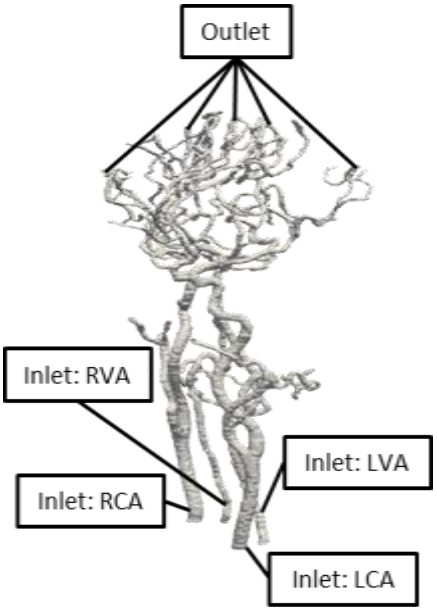

Fig. 6. Location of the boundary conditions for the cerebral artery at Inlet, Outlet and Wall

Table 1
Model coefficient of Eq. (14)

	A_{art}	β	a_0	a_1	a_2	a_3	a_4	b_1	b_2	b_3	b_4
LCA	4.52×10^{-5}	3.85×10^{-5}	0.260	-0.100	-0.101	-0.031	-0.014	0.169	-0.002	-0.002	-0.002
RCA	4.80×10^{-5}										
LVA	1.79×10^{-5}	3.77×10^{-5}									
RVA	1.51×10^{-5}										

2.3 Initial Conditions and Other Conditions
2.3.1 Initial conditions

The initial conditions for the pressure, the velocity and the virus concentration are explained. Regarding the nasal cavity and the cerebral artery, the pressure and the velocity fields need to be calculated. The pressure and the velocity fields of the nasal cavity and the cerebral artery are assumed to be 0 Pa and 0 m/s. The initial conditions of the virus concentration are explained. The virus concentration in the nasal cavity had been researched by CFD in considering with breathing waveform. As one period is a combination of exhalation and inhalation, it was found that the virus concentration is filled into all sinus after 10 periods. Figure 7 shows the virus concentration distribution in the nasal cavity, the organ and the cerebral artery after 10 periods. Initial virus concentration condition in the nasal cavity is used the virus concentration distribution as shown in Figure 7. Also, as initial virus concentration condition in the organ and cerebral artery is 0 mol/m^3.

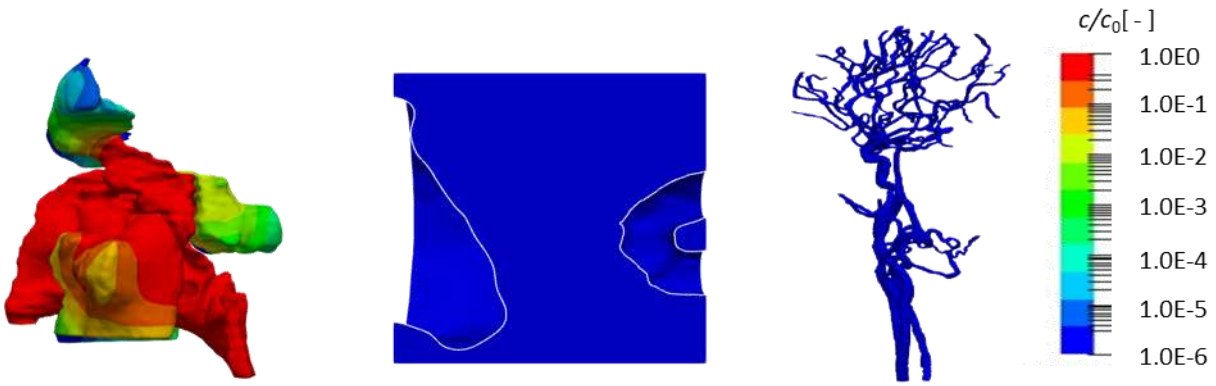

Fig. 7. Initial condition of pressure, velocity and concentration distribution

2.3.2 Other conditions

2.3.2.1 Breathing waveform in nasal cavity

The changed parameter is two which are the breathing waveform and the virus proliferation within the organ. Inlet velocity boundary in the nasal cavity is set up based on four types of the breathing waveform including steady with following equations,

simulated waveform:

$$Q_{nas}(t) = A_{nas}c_0\left\{1 + \sum_{i=1}^{7}\frac{c_i}{c_0}cos\left(2\pi i\frac{t}{T}\right) + \frac{b_i}{c_0}sin\left(2\pi i\frac{t}{T}\right)\right\} \quad (17)$$

sine function:

$$Q_{nas}(t) = A_{nas}\bar{u}_{nas}\left\{1 + \frac{u'_{nas}}{\bar{u}_{nas}}sin\left(2\pi i\frac{t}{T}\right)\right\} \quad (18)$$

$$\boldsymbol{u_{nas}}(r,t) = \frac{Q_{nas}(t)}{A_{nas}}\left(1 - \left(\frac{r}{R}\right)^2\right) \quad (19)$$

where $\bar{u}_{nas}$ is averaged velocity, T is period, A_{nas} is inlet area in the nasal cavity, c_i and d_i are model coefficient. Table 2 shows the model coefficient in the Eq. (17). Figure 8 shows the velocity breathing waveform in the nasal cavity. Figure 8(a) is Simulated Waveform with T=5.1 s, Figure 8(b) is sine function with T=5.1 s and Figure 8(c) is sine function with T=2.0 s. The averaged flow rate with each type waveform is same. We perform is total four case analysis in the nasal cavity which are the flow analysis based on these three types breathing waveforms and the steady flow analysis. Table 3 shows the all boundary condition of the nasal cavity, the organ, and the cerebral artery. Figure 9 shows the location relationships of boundary conditions between each model.

2.3.2.2 Virus proliferation in organ

Because the diffusion rate of virus concentration in the organ is generally slow, the virus proliferation within the organ needs to be considered. In this study, the infection in the first stage is assumed. Since the amount of virus proliferation is greater than the amount of virus killed by immunity system at the initial stage of infection, the effect of killed factor on the simulation result is small. Therefore, in the first stages of infection, the function for the amount of virus killed in the organ is simplified. Proliferation rate in Eq. (9) is defied under culture experiments in previous research by following equation,

$$f(t) = e^{\alpha t} \tag{20}$$

where α (=1.60×10^{-4}) is proliferation rate [33,34]. Figure 10 shows the time history of the number of virus within the organ.

Table 2
Model coefficient of Eq. (17)

A_{nas}	c_0	c_1	c_2	c_3	c_4	c_5	c_6	c_7
		1.597	-0.551	-0.523	-0.063	-0.036	-0.099	-0.018
1.31×10^{-4}	-0.080	d_1	d_2	d_3	d_4	d_5	d_6	d_7
		2.757	0.961	0.002	-0.108	0.064	-0.001	-0.031

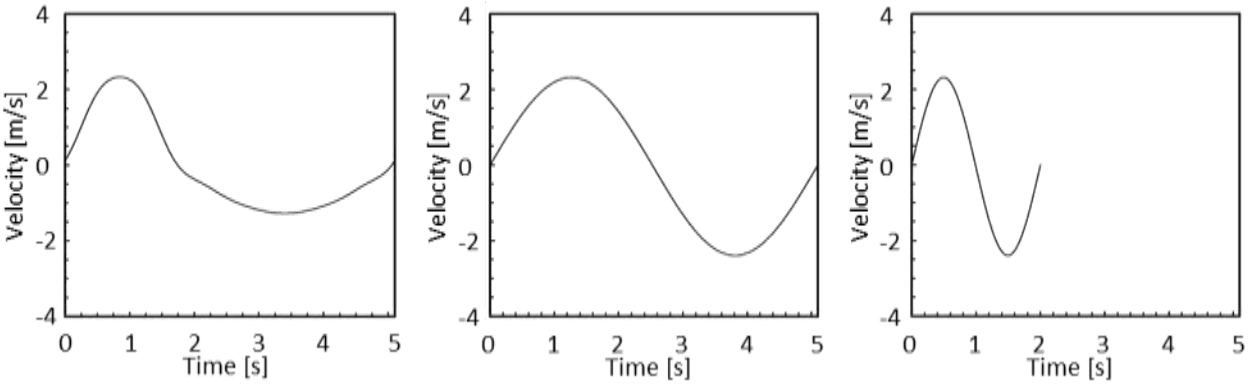

Fig. 8. Breathing waveform of inlet boundary condition in the nasal cavity, (a) Simulated Waveform (T=5.1 s), (b) Sine Function (T=5.1 s), (c) Sine Function (T=2.0 s)

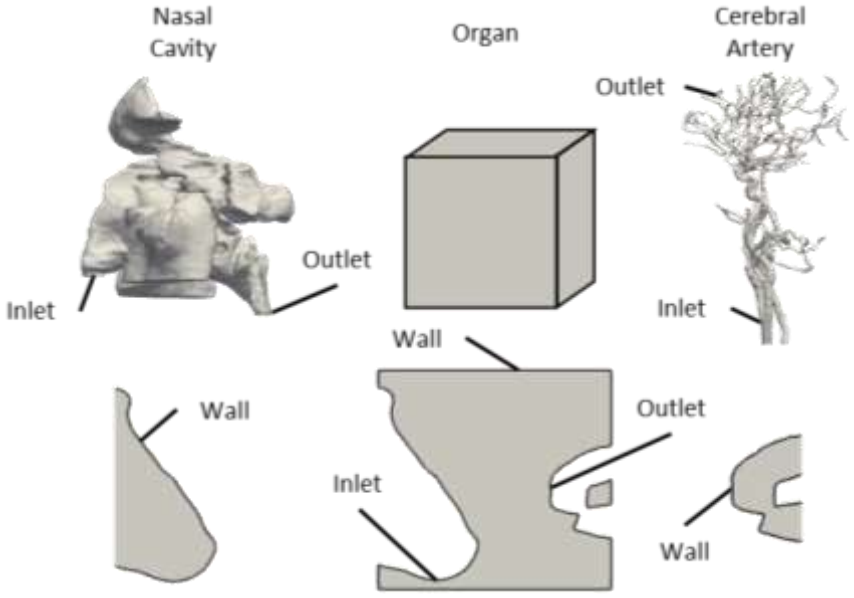

Fig. 9. Location relationships of boundary conditions between each model

Table 3
Boundary conditions at all geometries

			Velocity, Flow Rate	Pressure	Concentration
Nasal Cavity	Inlet BC	Steady	$Q_{nas}(t) = A_{nas}\bar{u}_{nas} = -5.37 \times 10^{-6}$	$\partial p_{nas}/\partial n = 0$	$\partial c_{nas}/\partial n = 0$
		Simulated Waveform (T=5.1 s)	$Q_{nas}(t) = A_{nas}c_0\left\{1 + \sum_{i=1}^{7}\frac{c_i}{c_0}cos\left(2\pi i\frac{t}{T}\right) + \frac{b_i}{c_0}sin\left(2\pi i\frac{t}{T}\right)\right\}$ Model coefficients are shown in Table 2		
		Sin Function (T=5.1 s)	$Q_{nas}(t) = A_{nas}\bar{u}_{nas}\left\{1 + \frac{u'_{nas}}{\bar{u}_{nas}}sin\left(2\pi i\frac{t}{T}\right)\right\}$ ※$\frac{u'_{nas}}{\bar{u}_{nas}} = 57.42$		
		Sin Function (T=2.0 s)			
	Outlet BC	Steady	$\partial \boldsymbol{u}_{nas}/\partial n = 0$	$p_{nas} = 0$	$\partial c_{nas}/\partial n = 0$
		Simulated Waveform (T=5.1 s)			
		Sin Function (T=5.1 s)			
		Sin Function (T=2.0 s)			
	Wall BC	Steady	$\boldsymbol{u}_{nas} = 0$	$\partial p_{nas}/\partial n = 0$	$\partial c_{nas}/\partial n = -k_{coff}c_{nas}/D_{m,n}$
		Simulated Waveform (T=5.1 s)			
		Sin Function (T=5.1 s)			
		Sin Function (T=2.0 s)			
Organ	Inlet BC		-	-	$c_{org} = T_{org}c_{nas}$
	Wall BC		-	-	$\partial c_{org}/\partial n = 0$
	Outlet BC		-	-	$\partial c_{org}/\partial n = 0$
Cerebral Artery	Wall BC		$\boldsymbol{u}_{art} = 0$	$\partial p_{art}/\partial n = 0$	$c_{art} = T_{art}c_{org}$
	Inlet BC		$Q_{art}(t) = A_{art}\beta\left\{a_0 + \sum_{i=1}^{4}a_i\,cos\left(\frac{2\pi i}{T}t\right) + b_i\,sin\left(\frac{2\pi i}{T}t\right)\right\}$ (T=0.8 s) Model coefficients are shown in Table 1	$\partial p_{art}/\partial n = 0$	$\partial c_{art}/\partial n = 0$
	OutletBC		$\partial \boldsymbol{u}_{art}/\partial n = 0$	$p_{art} = 0$	$\partial c_{art}/\partial n = 0$

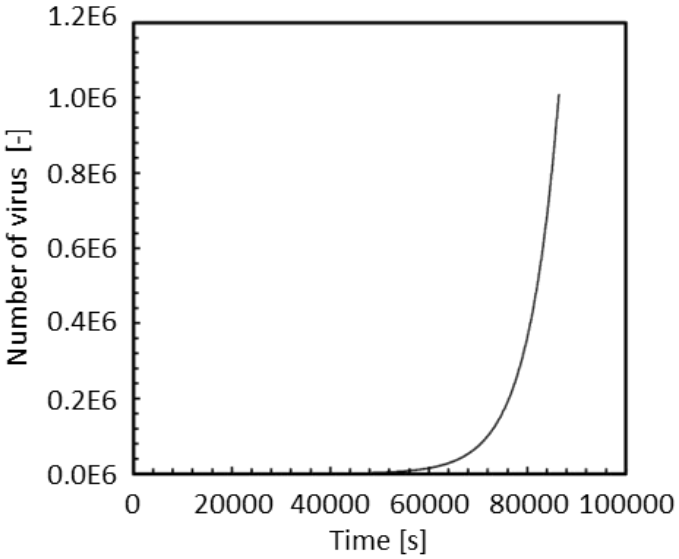

Fig. 10. Time history of number of virus within the organ

3. Results and Discussions

3.1 Transport Route Based on Virus Concentration Distribution

The virus transport process from the nasal cavity to the cerebral artery is explained by the results of steady analysis. The virus concentration in the nasal cavity and the organ is investigated. Figure 11 shows the virus concentration distribution in the nasal cavity and the organ at 20 s to 100 s. Furthermore, the virus concentration distributions are dimensionless by using the standard virus concentration (c_0 = 4.98×10^{-11} mol/m^3). Since the virus concentration is flowed the airways into the sinus by breathing, the virus concentration in the sinus increases. However, diffusion rate of the virus concentration in the organ is slower than in the nasal cavity. Generally, since the diffusion coefficient in the organ is extremely small, it is necessary for the virus concentration transport in the organ to be for several days. Figure 12 shows the virus concentration distribution in the organ. The virus concentration flowed from the nasal cavity reach to the cerebral artery for 12 hours. Since general incubation period of the virus is 3days, the virus concentration transport analysis in the organ is calculated during 3 days. The virus concentration distributions in the cerebral artery after 3 days from the virus inflow into the nasal cavity are investigated. Figure 13 shows the virus concentration distribution in the cerebral artery. After the virus concentration stay in the contact surface between the organ and the cerebral artery for few minutes, the virus concentration is transported to the downstream of the cerebral artery for approximately four minutes. Figure 14 shows the virus concentration distribution from the nasal cavity to the cerebral artery after 24 hours. Since the geometries of the nasal cavity and the cerebral artery is asymmetrical with left and right, it is greatly differed: the surface area in contact with the organ, and the distance between the nasal cavity and the cerebral artery. In these geometries, since the left side sphenoid sinus is larger than right side one, it has the characteristic that the virus concentration is likely to be flowed into the left side. In addition, because the distance between left side sphenoid sinus and the cerebral artery is closed, it can be seen that most of the virus concentration is transported to the cerebral artery via the left sphenoid sinus. Furthermore, since the diameter of the left side cerebral artery is larger than right side, the surface area in contact with the virus concentration at the left side cerebral artery is larger than right side one. It was suggested that there is a bias of the virus concentration distribution results in the cerebral arteries due to left-right asymmetry of the geometries.

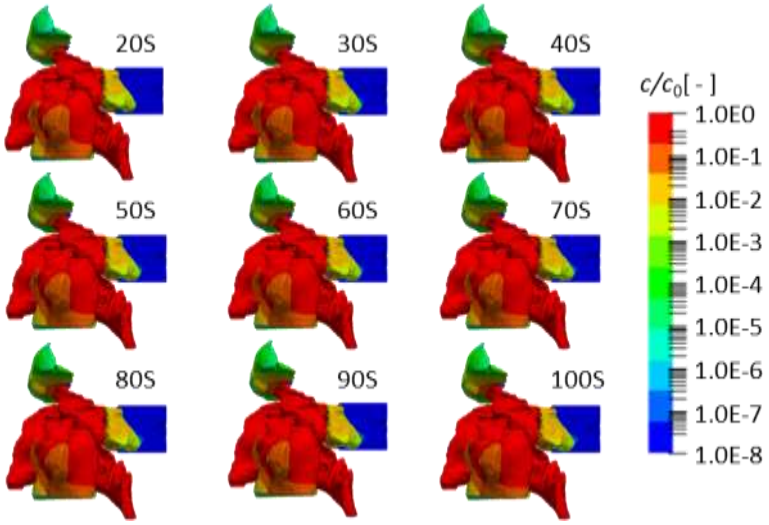

Fig. 11. Concentration distribution in the nasal cavity and the organ with Steady (Since time reached to the organ t = 20 s ~ 100 s)

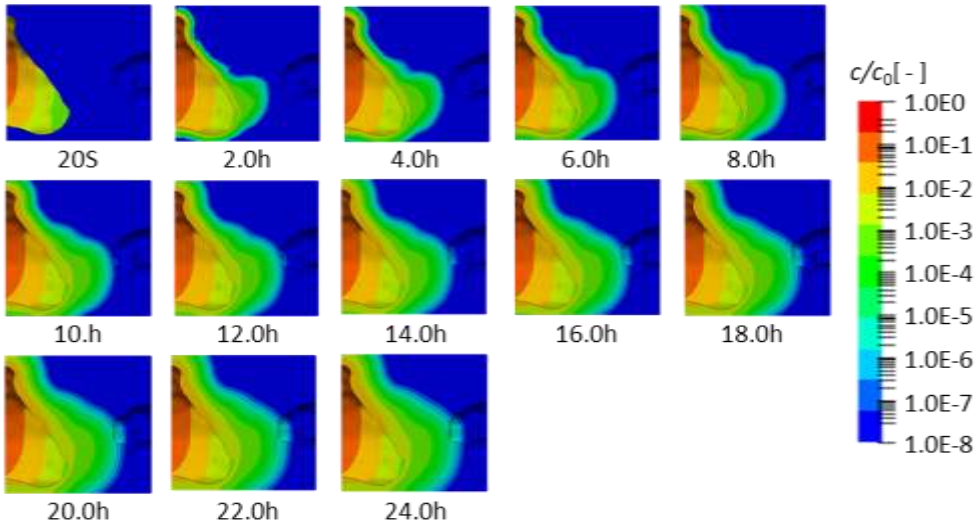

Fig. 12. Concentration distribution in the organ with Steady (Since time reached to the organ t = 20s ~ 24h)

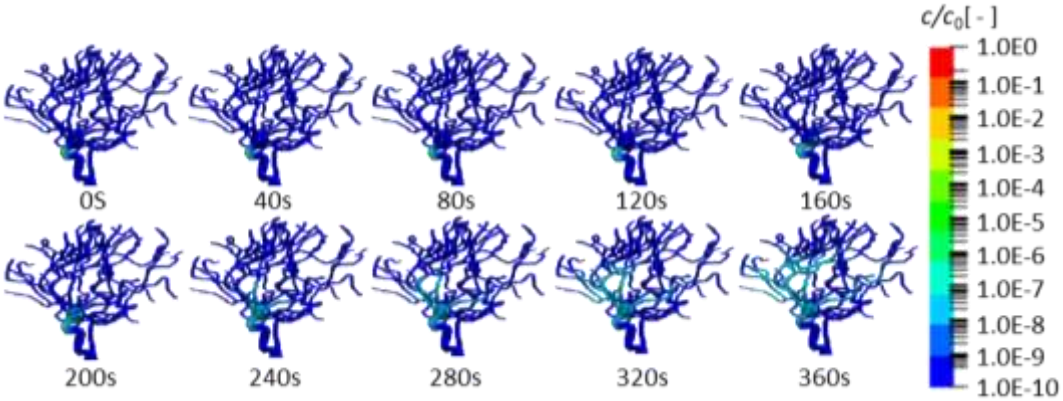

Fig. 13. Concentration distribution in the cerebral artery with steady (Since time reached to the cerebral artery t = 0 s ~ 360 s)

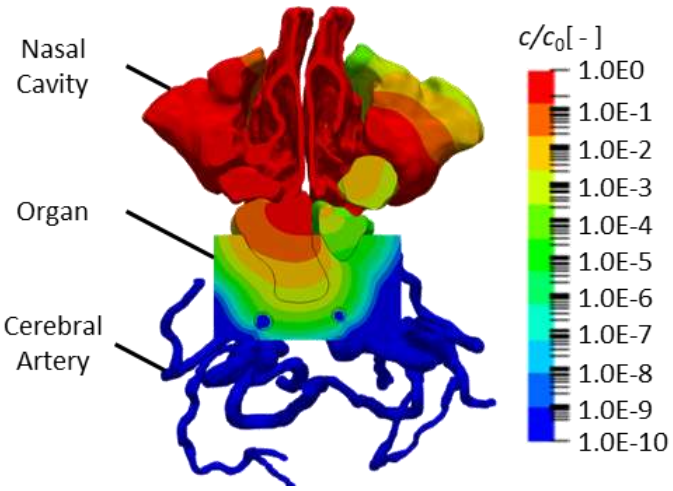

Fig. 14. Concentration distribution from the nasal cavity to the cerebral artery (Since time reached to the organ t = 24 h)

3.2 Comparison of Volume-Averaged Virus Concentration Due to Differences in Breathing Waveform

Effects of the virus concentration on the changes of the breathing waveform in the nasal cavity is investigated. Firstly, the time history of the volume-averaged virus concentration in the nasal cavity is compared with 3 types of the breathing waveform and steady flow. The volume-averaged virus concentration in the sphenoid sinus is calculated. Figure 15 shows the region measured the time history of the volume-averaged virus concentration in the nasal cavity, the organ and the cerebral artery. The volume-averaged virus concentration is defined by following equation,

$$\overline{(c/c_0)}_i = \frac{1}{V_i}\int_{V_i}\frac{c}{c_0}dV_i \tag{21}$$

where V is the volume in the measurement regions. Figure 16 shows the time history of the volume-averaged virus concentration in the nasal cavity. It was seen the volume-averaged virus concentration in the sphenoid sinus increases with all types of breathing waveform. First, the volume-averaged virus concentration is compared the simulated waveform (T=5.1s) with the sine function (T=5.1s). The difference of 2 types of breathing waveform is a ratio of inhalation time on exhalation time. The averaged flow rate of both breathing waveforms is same. In comparison with both breathing waveforms, it was found that the virus concentration with the sine function is more likely to be stayed than with the simulated waveform. In other words, even if the averaged flow rate in one period is same, it was found that the breathing waveform with a long exhalation time compared with inhalation time causes the virus concentration to be not likely to stay in the sinuses. Second, the effect of the volume-averaged virus concentration on the change of period is evaluated. In comparison long period's waveform with short period's waveform, it was found that the virus concentration with long period's waveform is more likely to be stayed than with short period's waveform. Therefore, it was suggested that the risk of infection in the sinus decrease by speed up the breathing period and lengthen the exhaust time of the breathing waveform.

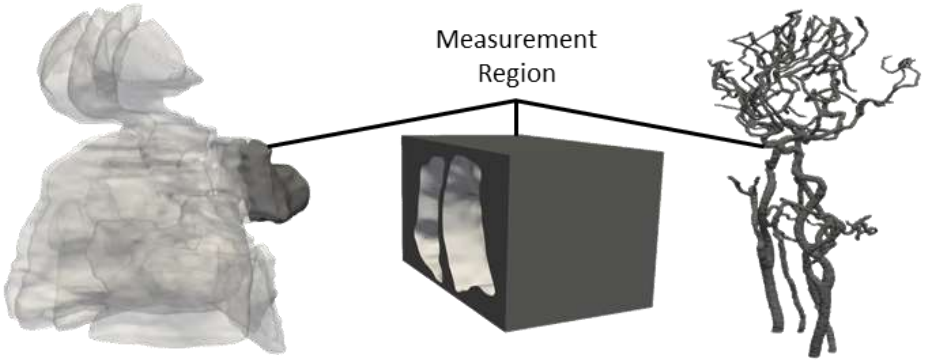

Fig. 15. Measurement region of the time history of volume-averaged virus concentration

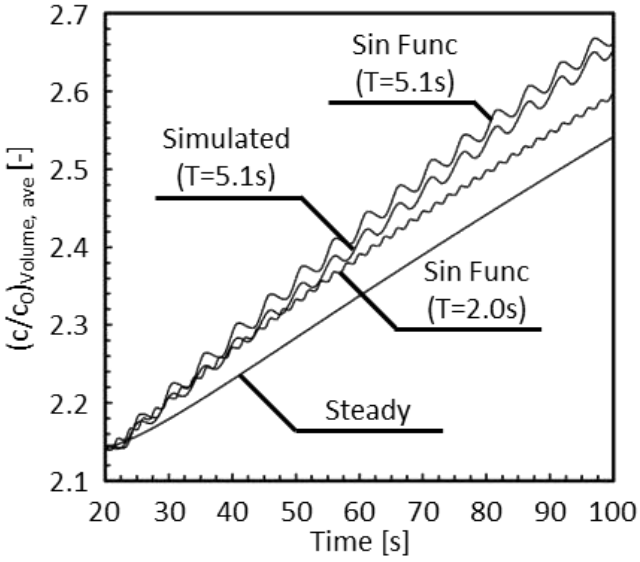

Fig. 16. Time history of volume-averaged virus concentration in the nasal cavity (Since time reached to the organ t = 20 s ~ 100 s)

Figure 17 shows the time history of the volume-averaged virus concentration in the organ. Although The volume-averaged virus concentration in nasal cavity with the sine function (T=5.1s) is largest, the volume-averaged virus concentration in organ with the sine function (T=2.0s) is largest. It can be expected that there is the difference between the virus concentration in the fluid and the virus concentration near the wall. Figure 18 shows the difference of the virus concentration distribution in the organ at t = 86120s. Figure 18(a) shows the difference between Simulated (T=5.1s) and Steady. Figure 18(b) shows the difference between sine function (T=5.1s) and Steady. Figure 18(c) shows the difference between sine function (T=2.0s) and Steady. The difference in the virus concentration distribution in the organ was calculated based on the steady calculation results. The virus concentration distribution on the wall of the sphenoid sinus is changed in the difference of the breathing waveform, and it can be seen that the virus concentration flowed into the organ from the nasal cavity is larger in case of sine function (T=2.0s) than in case of sine function (T=5.1s). Figure 19 shows the time history of the volume-averaged virus concentration in the cerebral artery. As time passes, the virus concentration in the carotid artery decreases. The reason is that the virus concentration is transported downstream of the cerebral arteries and flows out into the cerebral veins. Figure 20 shows the difference of the virus concentration distribution in the cerebral artery at t = 86120s. Figure 20(a) shows the difference between Simulated (T=5.1s) and Steady. Figure 20(b)

shows the difference between sine function (T=5.1s) and Steady. Figure 20(c) shows the difference between sine function (T=2.0s) and Steady. The difference in the virus concentration distribution in the cerebral artery was calculated based on the steady calculation results. The virus concentration distribution on the wall of the cerebral artery is changed in the difference of the breathing waveform.

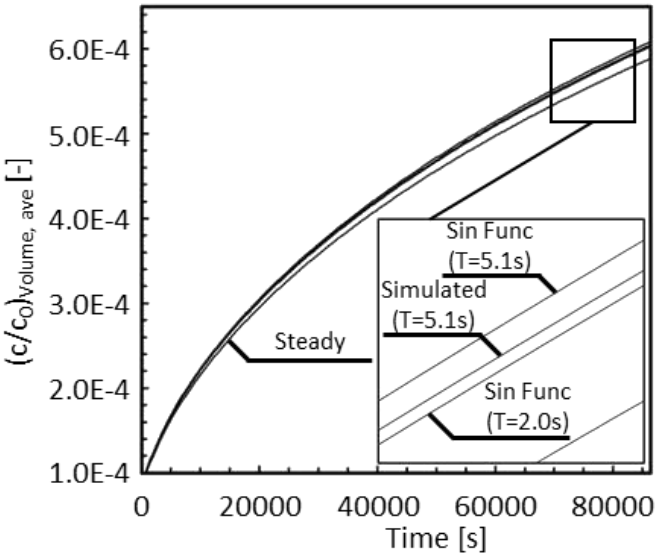

Fig. 17. Time history of volume-averaged virus concentration in the organ (Since time reached to the organ t = 20 s ~ 86120 s)

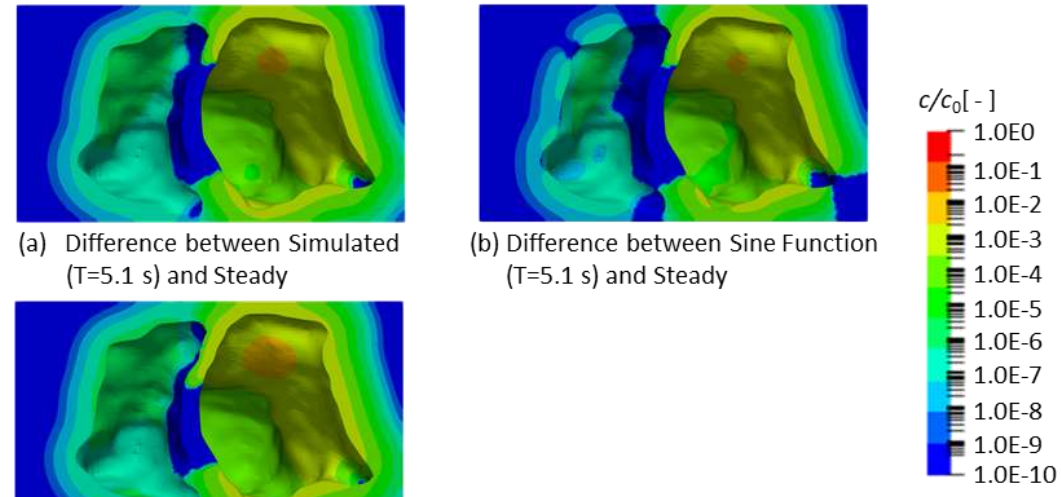

(a) Difference between Simulated (T=5.1 s) and Steady

(b) Difference between Sine Function (T=5.1 s) and Steady

(c) Difference between Sine Function (T=2.0 s) and Steady

Fig. 18. Difference of the virus concentration distribution in the organ (Since time reached to the organ t = 86120 s)

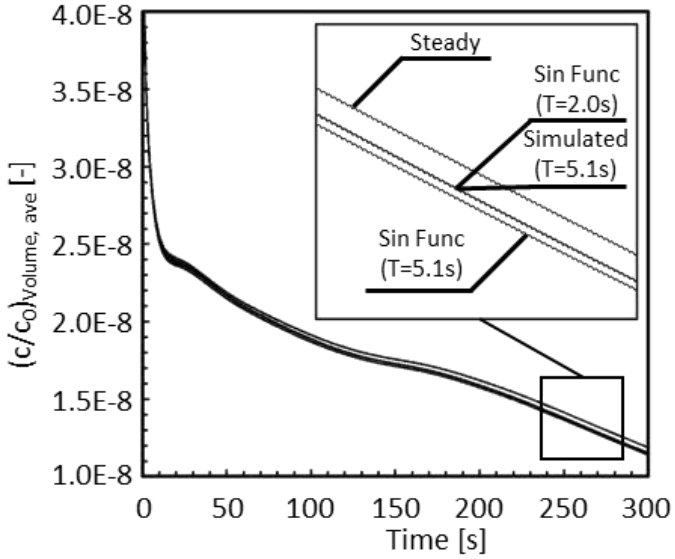

Fig. 19. Time history of volume-averaged virus concentration in the cerebral artery (Since time reached to the cerebral artery t = 0 s ~ 300 s)

Fig. 20. Difference of the virus concentration distribution in the cerebral artery (Since time reached to the organ t = 86120 s)

In order to check tendencies of the region to be likely stay the virus concentration reached to the cerebral artery, the cerebral artery is divided into 6parts, and the time history of the volume-averaged virus concentration is compared with these parts. Figure 21 shows the schematic diagram of cerebral artery divided into 6 parts. The virus concentration from the organ is flowed to LCA, RCA and Front CBA. Figure 22 shows the time history of virus concentration each part at Steady. It was found that the virus concentration at the Front CBA becomes to be largest. The reason is that the location of Front CBA is the confluence part of virus concentration. It is suggested that the possible of the inflammatory reactions in these parts is high. It can be seen that the virus concentration is transported to LBA, RBA, and Back CBA as time passes. Figure 23 shows the time history of the ratio of the virus concentration in each region to in the total region at Steady. Figure 24 shows the ratio of the virus concentration in each region to in the total region at t = 300 s. It was found that the virus

concentration at the Front CBA becomes to be largest. It was found that the bias of the ratio of virus concentration in the cerebral arteries due to left-right asymmetry of the geometries.

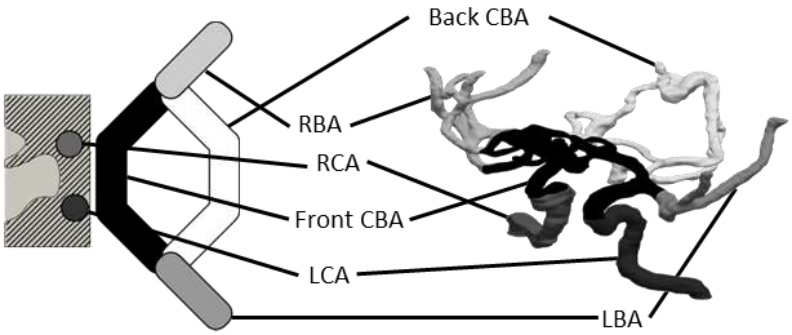

Fig. 21. Schematic diagram of cerebral artery divided into 6 parts

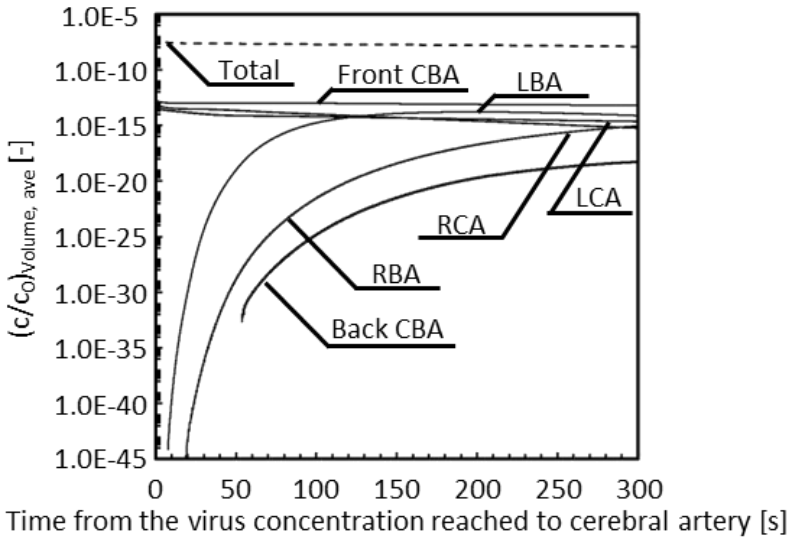

Fig. 22. Time history of virus concentration in the cerebral artery with Steady (Since time reached to the cerebral artery t = 0 s ~ 300 s)

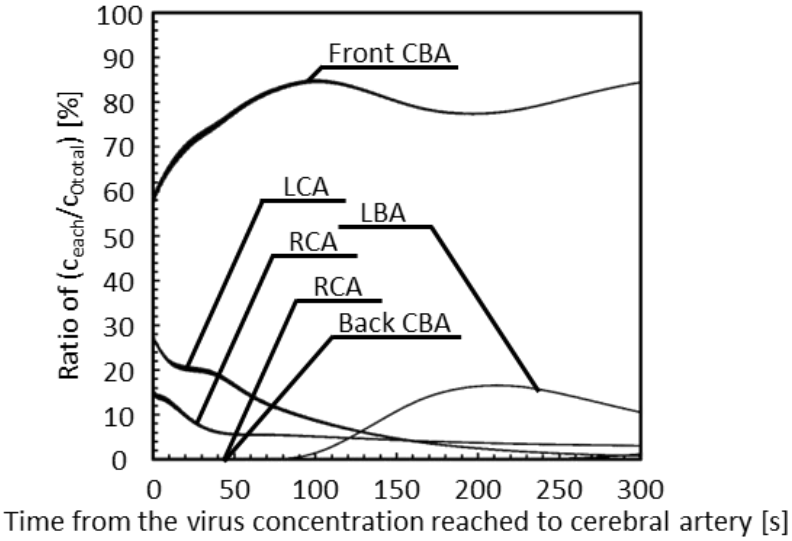

Fig. 23. Time history of rate of concentration in each region to the total region with Steady (Since time reached to the cerebral artery t = 0 s ~ 300 s)

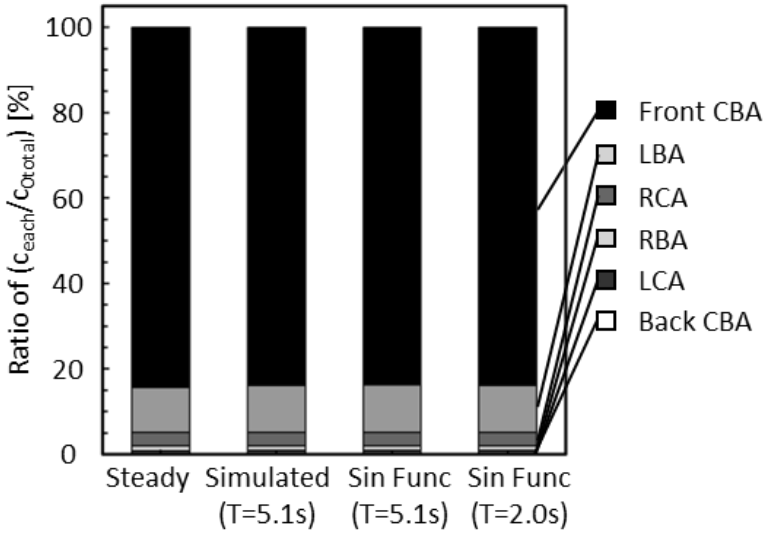

Fig. 24. Rate of concentration in each region to the total region with Steady (Since time reached to the cerebral artery t = 300 s)

3.3 Comparison of Time-Volume-Averaged Virus Concentration Due to Differences in Breathing Waveform and Proliferation

As shown in Figure 12, since the speed of the virus concentration diffusion in the organ is extremely slow, there is generally a possibility that viruses proliferate during movement in the organ. The effect of the proliferation or not on the virus concentration distribution in the organ and the cerebral artery is investigated by using the virus concentration distribution, and they are compared with the differences in the breathing waveform and the proliferation or not using time-volume-averaged virus concentration.

Figure 25 shows the virus concentration distribution in the organ in consideration with proliferation. When compared with no-proliferation in Figure 12, the virus concentration distribution with proliferation is higher than the no- proliferation. Figure 26 shows the virus concentration distribution in the cerebral artery in consideration with proliferation. The virus concentration in the cerebral artery becomes to increase by considering with the proliferation. When considering the proliferation of the virus, it can be seen that a high concentration of virus reaches the downstream side of the cerebral artery. It was suggested that when the virus proliferates explosively within the organ, the risk of virus infection is increased by spreading the virus concentration throughout the cerebral artery.

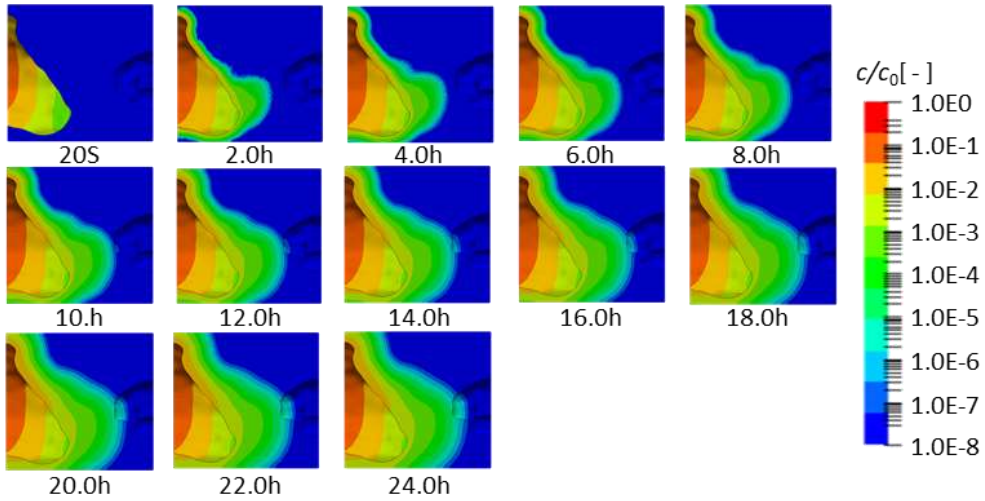

(a)

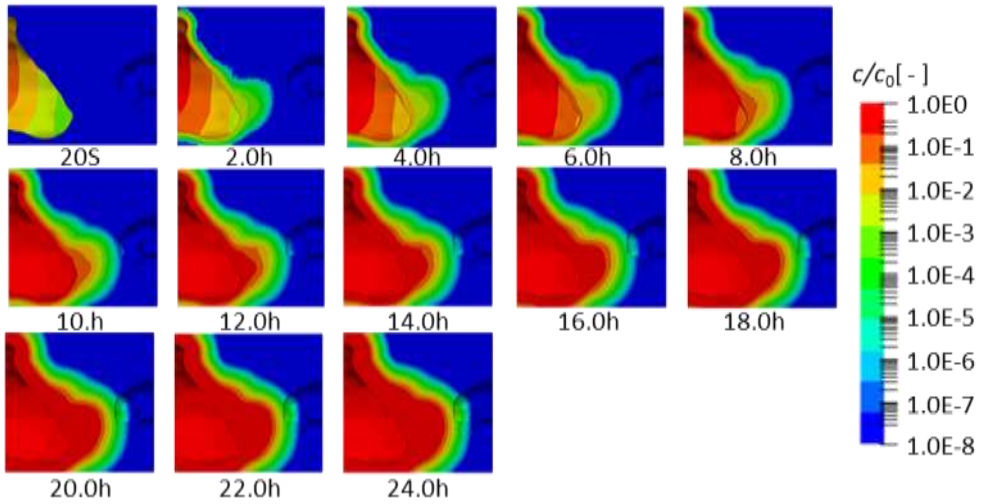

(b)

Fig. 25. Concentration distribution in the organ in consideration with proliferation with Steady (Since time reached to the organ t = 20 s ~ 24 h), (a) Turn off the proliferation using Eq. (8) (Figure 12), (b) Turn on the proliferation using Eq. (9)

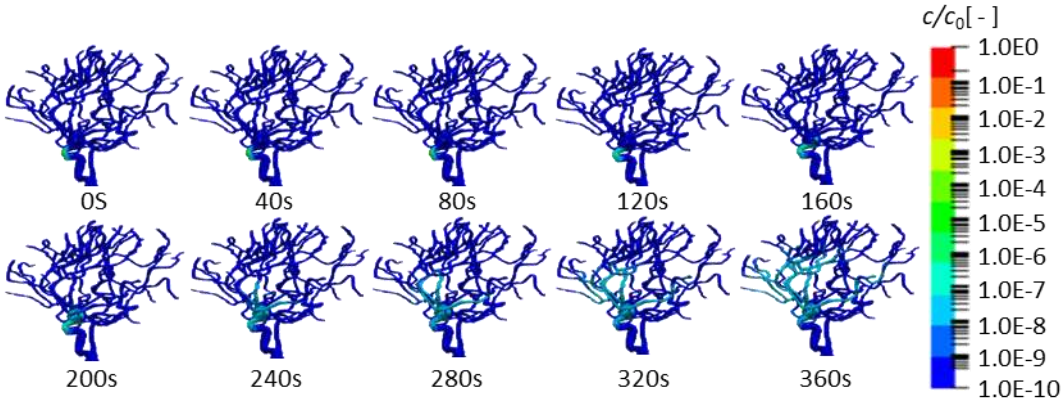

(a)

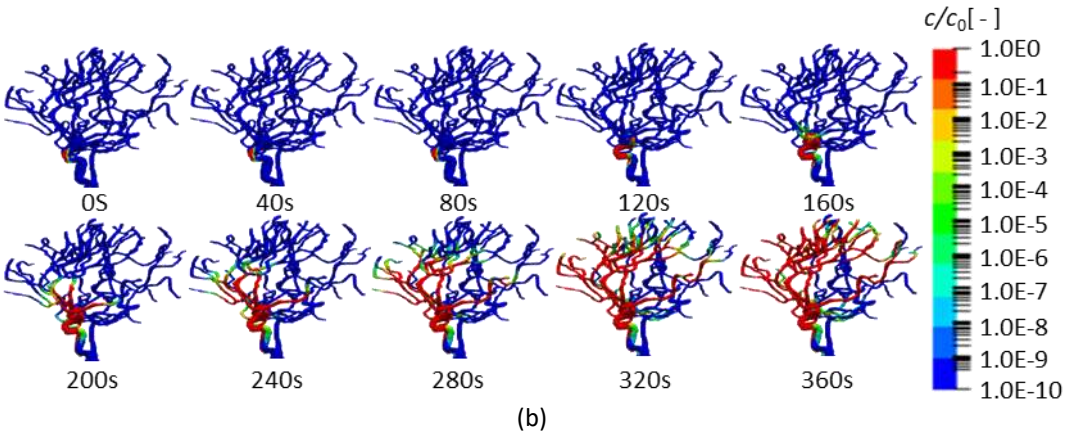

(b)

Fig. 26. Concentration distribution in the cerebral artery in consideration with proliferation with Steady (Since time reached to the cerebral artery t = 0 s ~ 360 s) (a) Turn off the proliferation using Eq. (8) (Figure 13), (b) Turn on the proliferation using Eq. (9)

In order to investigate the rate of the virus concentration reached to the cerebral artery on the virus concentration flowed into the nasal cavity, the time-volume-averaged virus concentration is calculated. The time-volume averaged virus concentration in each breathing waveform is normalized by the value of the nasal cavity. The time-volume-averaged virus concentration is defined by following equation.

$$\overline{(c/c_0)}_{time,i} = \frac{1}{T}\int_0^T \left(\frac{1}{V_i}\int_{V_i} \frac{c}{c_0} dV_i\right) dt = \frac{1}{T}\int_0^T \overline{(c/c_0)}_i dt \tag{22}$$

Figure 27 shows the time-volume-averaged virus concentration in the nasal cavity, the organ and the cerebral artery with each breathing waveform. In case of the no-proliferation, as the virus concentration in the nasal cavity is largest, the virus concentration in the organ and cerebral artery decrease. It was found that the virus concentration reached to the cerebral artery is 10-8 times as much as the virus concentration in the nasal cavity. In this research, it was assumed to be that all transmission rate of virus concentration is 1. Therefore, since the transmission rate in vivo is smaller than this analysis case, it was considered that the virus concentration reached to the cerebral artery is smaller than this analysis case. In case of the proliferation, the virus concentration in the cerebral artery is largest. It was found that the virus concentration reached to the cerebral artery is 2×104 times as much as the virus concentration in the nasal cavity.

In order to investigate the difference of the virus concentration each breathing waveform, the ratio of the virus concentration reached to the cerebral artery to the virus concentration flowed into the nasal cavity are evaluated. Figure 28 shows the ratio of the virus concentration in the cerebral artery to the nasal cavity. Regardless of the proliferation or not, the ratio of the virus concentration is largest in Steady, and the ratio of the virus concentration is smallest in sine function with long period. In other words, the breathing methods which the effect of the virus concentration proliferation or not is smallest, is sine function with long period. It was found that the risk of infection in the sinus decrease by speed up the breathing period and lengthen the exhaust time of the breathing waveform.

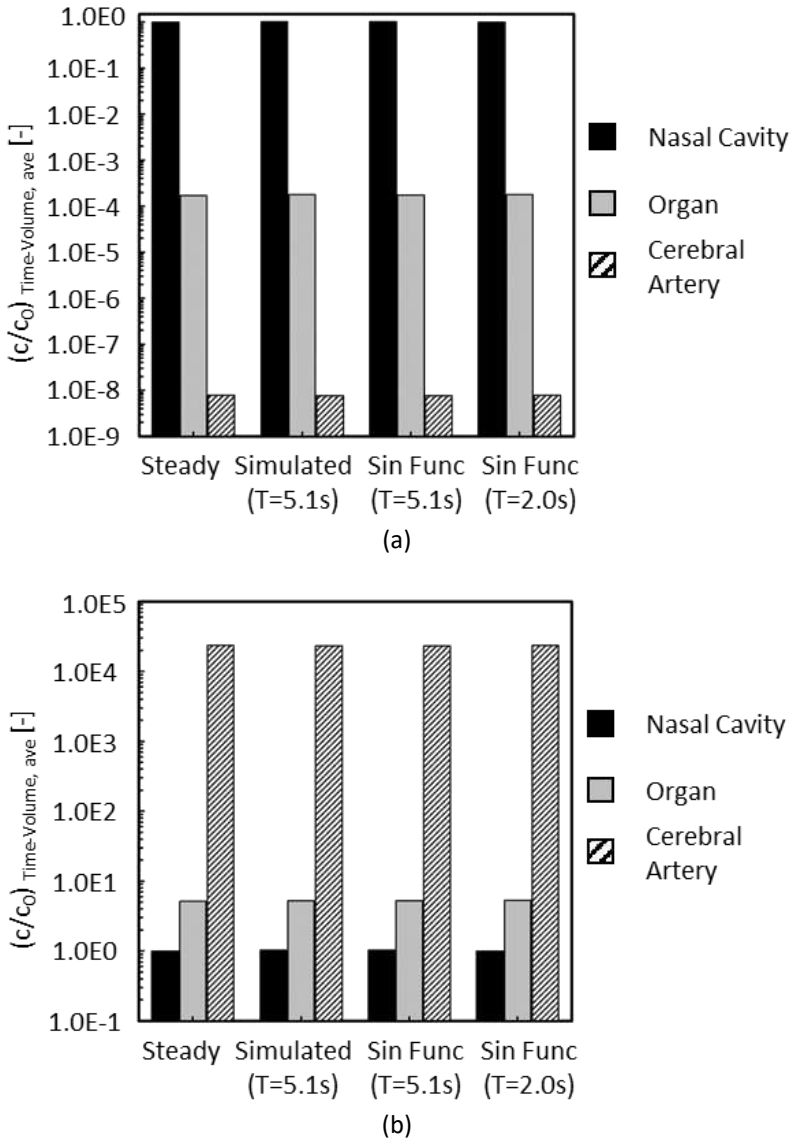

Fig. 27. Time-Volume-averaged virus concentration, (a) Turn off the proliferation using Eq. (8), (b) Turn on the proliferation using Eq. (9)

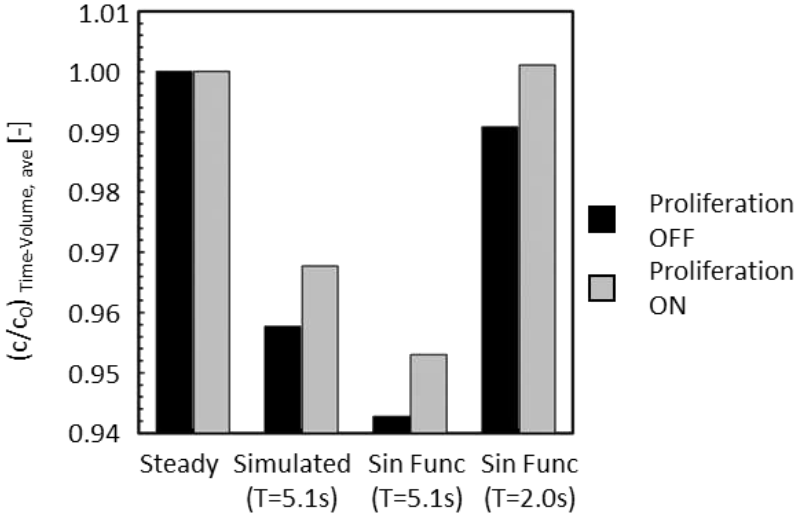

Fig. 28. Ratio of the concentration in the cerebral artery to the nasal cavity

4. Limitation

A method for simulating viral infection from the nasal cavity to the cerebral artery was proposed. But this study has some limitation. This research is needed to be considered the parameter like transmission rate on the boundary condition, virus proliferation rate within the tissues and the clinical pressure waveforms and respiratory waveforms. This study proposed a method for simulating the virus transport process from the nasal cavity to the cerebral arteries, and investigated the effects of breathing waveforms and virus proliferation within the organ by using simplified parameters.

Therefore, in order to clarify the mechanism of virus infection in vivo, it is necessary to identify parameters by comparing clinical data with simulation results. A lot of clinical data is required to identify parameters. In this study, because there is not enough clinical data to identify parameters such as transmission rate and breathing waveforms, the details of parameters have not been analysed.

5. Conclusion

In this research, a couple analysis from nasal cavity to cerebral artery via organ was tried to be applied in order to analyze the transport process of them. The effect of breathing waveforms and virus proliferation on the virus infection is evaluated. The obtained conclusions are shown below.

i) The virus concentration in the cerebral artery in case of sinusoidal breathing waveform with long period is the smallest.
ii) The virus concentration in the organ and the cerebral artery in case of proliferation within the organ is higher than that has no proliferations.
iii) The highest risk of the virus infection in the cerebral artery was the joint with the left and right carotid arteries.

In the future, we will establish an optimal virus infection model by changing various parameters such as transmittance and comparing with clinical data. In addition, in order to clarify the differences in virus stayed positions due to differences of geometries, we plan to apply this method to different geometries, and compare them.

Acknowledgement

This study was partially supported by Co-Funding Research Program established between Kyushu Institute of Technology (KYUTECH) and Universiti Putra Malaysia (UPM) and JST SPRING, Japan Grant Number JPMJSP2154.

References

[1] Zhang, Zhihang, Taehoon Han, Kwang Hee Yoo, Jesse Capecelatro, André L. Boehman, and Kevin Maki. "Disease transmission through expiratory aerosols on an urban bus." *Physics of Fluids* 33, no. 1 (2021). https://doi.org/10.1063/5.0037452

[2] Kohanski, Michael A., L. James Lo, and Michael S. Waring. "Review of indoor aerosol generation, transport, and control in the context of COVID-19." In *International forum of allergy & rhinology*, vol. 10, no. 10, pp. 1173-1179. 2020. https://doi.org/10.1002/alr.22661

[3] Noorimotlagh, Zahra, Neemat Jaafarzadeh, Susana Silva Martínez, and Seyyed Abbas Mirzaee. "A systematic review of possible airborne transmission of the COVID-19 virus (SARS-CoV-2) in the indoor air environment." *Environmental research* 193 (2021): 110612. https://doi.org/10.1016/j.envres.2020.110612

[4] Rowe, Bertrand R., André Canosa, Jean-Michel Drouffe, and James Brian Alexander Mitchell. "Simple quantitative assessment of the outdoor versus indoor airborne transmission of viruses and COVID-19." *Environmental research* 198 (2021): 111189. https://doi.org/10.1016/j.envres.2021.111189

[5] Bazant, Martin Z., Ousmane Kodio, Alexander E. Cohen, Kasim Khan, Zongyu Gu, and John WM Bush. "Monitoring carbon dioxide to quantify the risk of indoor airborne transmission of COVID-19." *Flow* 1 (2021): E10. https://doi.org/10.1017/flo.2021.10

[6] Wu, Hsiu, Minn M. Soe, Rebecca Konnor, Raymund Dantes, Kathryn Haass, Margaret A. Dudeck, Cindy Gross et al. "Hospital capacities and shortages of healthcare resources among US hospitals during the coronavirus disease 2019 (COVID-19) pandemic, National Healthcare Safety Network (NHSN), March 27–July 14, 2020." *Infection Control & Hospital Epidemiology* 43, no. 10 (2022): 1473-1476. https://doi.org/10.1017/ice.2021.280

[7] Soyemi, Toluwalashe Sogbenga, and Abdullahi Tunde Aborode. "Shortage of hospital bed capacity and overcrowding in emergency tertiary healthcare centers in Nigeria." *Annals of Medicine and Surgery* 82 (2022). https://doi.org/10.1016/j.amsu.2022.104675

[8] Gubler, Duane J. "Dengue and dengue hemorrhagic fever." *Clinical microbiology reviews* 11, no. 3 (1998): 480-496. https://doi.org/10.1128/CMR.11.3.480

[9] Feng, Kaishan, Yoshiki Yanagita, Yuko Miyamura, Adi Azriff Basri, Mohammad Zuber, Siti Rohani, Kamarul Arifin Ahmad, and Masaaki Tamagawa. "CFD Analysis of Indoor Ventilation for Airborne Virus Infection." *Journal of Advanced Research in Numerical Heat Transfer* 14, no. 1 (2023): 1-16. https://doi.org/10.37934/arnht.14.1.116

[10] Kaishan, Feng, Yanagita Yoshiki, Miyamura Yuko, Basri Adi Azriff, Zuber Mohammad, Rohani Siti, Aziz Abdul, Ahmad Kamarul Arifin, and Tamagawa Masaaki. "Fundamental Investigation on Ventilation Methods of Indoor Air for Preventing Infections by Computational Fluid Dynamics Analysis." *ICIC Express Letters* 17, no. 10 (2023): 1103. https://doi.org/10.24507/icicel.17.10.1103

[11] Dai, Hui, and Bin Zhao. "Association of the infection probability of COVID-19 with ventilation rates in confined spaces." In *Building simulation*, vol. 13, pp. 1321-1327. Tsinghua University Press, 2020. https://doi.org/10.1007/s12273-020-0703-5

[12] Eames, Ian, J. W. Tang, Y. Li, and P. Wilson. "Airborne transmission of disease in hospitals." *Journal of the Royal Society Interface* 6, no. suppl_6 (2009): S697-S702. https://doi.org/10.1098/rsif.2009.0407.focus

[13] Liu, Li, Yuguo Li, Peter Vilhelm Nielsen, Jianjian Wei, and Rasmus Lund Jensen. "Short-range airborne transmission of expiratory droplets between two people." *Indoor air* 27, no. 2 (2017): 452-462. https://doi.org/10.1111/ina.12314

[14] Kassem, Fatma AbdelMordy. AbdelGawad, Ahmed Farouk. Abuel-Ezz, Ali Elsayed. Nassief, Mofreh Melad. Adel, Mohamed. "Design and Performance Evaluation of a Portable Chamber for Prevention of Aerosol Airborne – Infection." *Journal of Advanced Research in Fluid Mechanics and Thermal Sciences* 100, issue 2 (2022): 181-197. https://doi.org/10.37934/arfmts.100.2.181197

[15] El-Haroun, Ahmed Fahmy. Kaseb, Sayed Ahmed. Fouad, Mahmoud Ahmed. Kayed, Hatem Omar. "Numerical Investigation of Covid-19 Infection Spread Expelled fromCough in an Isolation Ward Under Different Air Distribution Strategies." *Journal of Advanced Research in Fluid Mechanics and Thermal Sciences* 95, issue 1 (2022): 17-35. https://doi.org/10.37934/arfmts.95.1.1735

[16] Yanagita, Yoshiki. Feng, Kaishan. Miyamura, Yuko. Basri, Adi Azriff. Zuber, Mohammd. Rohani, Siti. Aziz, Abdul. Ahmad, Kamarul Arifin. Tamagawa, Masaaki. "Evaluation of Virus Concentration Analysis in the Airway by CFD." *Journal of Advanced Research in Numerical Heat Transfer* 13, no. 1 (2023): 96-105. https://doi.org/10.37934/arnht.13.1.96105

[17] Farnoud, Ali, Ingo Baumann, Mohammad Mehdi Rashidi, Otmar Schmid, and Eva Gutheil. "Simulation of patient-specific bi-directional pulsating nasal aerosol dispersion and deposition with clockwise 45 and 90 nosepieces." *Computers in Biology and Medicine* 123 (2020): 103816. https://doi.org/10.1016/j.compbiomed.2020.103816

[18] Li, Chengyu. Jiang, Jianbo. Dong, Haibo. Zhao, Kai. "Computational modeling and validation of human nasal airflow under various breathing conditions." *Journal of Biomechanics* 64, no.7 (2017): 59-68. https://doi.org/10.1016/j.jbiomech.2017.08.031

[19] Zhao, Kai, Pamela Dalton, Geoffery C. Yang, and Peter W. Scherer. "Numerical modeling of turbulent and laminar airflow and odorant transport during sniffing in the human and rat nose." *Chemical senses* 31, no. 2 (2006): 107-118. https://doi.org/10.1093/chemse/bjj008

[20] Inthavong, Kiao, Jiawei Ma, Yidan Shang, Jingliang Dong, Annicka SR Chetty, Jiyuan Tu, and Dennis Frank-Ito. "Geometry and airflow dynamics analysis in the nasal cavity during inhalation." *Clinical Biomechanics* 66 (2019): 97-106. https://doi.org/10.1016/j.clinbiomech.2017.10.006

[21] Brüning, Jan, Thomas Hildebrandt, Werner Heppt, Nora Schmidt, Hans Lamecker, Angelika Szengel, Natalja Amiridze et al. "Characterization of the airflow within an average geometry of the healthy human nasal cavity." *Scientific reports* 10, no. 1 (2020): 3755. https://doi.org/10.1038/s41598-020-60755-3

[22] Yu, Shen. Wang, Danqing. Guo, Yan. Shen, Shuang. Wang, Jizhe. "Numerical Study on the Distribution of Nitric Oxide Concentration in the Nasal Cavity of Healthy People during Breathing." *Nitric Oxide* 130 (2023): 12–21. https://doi.org/10.1016/j.niox.2022.11.002

[23] Corda, John Valerian, B. Satish Shenoy, Leslie Lewis, Prakashini K, SM Abdul Khader, Kamarul Arifin Ahmad, and Mohammad Zuber. "Nasal airflow patterns in a patient with septal deviation and comparison with a healthy nasal cavity using computational fluid dynamics." *Frontiers in Mechanical Engineering* 8 (2022): 1009640. https://doi.org/10.3389/fmech.2022.1009640

[24] Zuber, Mohammad, Kamarul Arifin Ahmad, SM Abdul Khader, R. Balakrishnan, Sharath Honnani, Sana Althaf Hussain, and A. B. V. Barboza. "Effect of Septum Deviation on the Airflow Distribution for a Patient Specific Model using Numerical Methods." *Journal of Advanced Research in Numerical Heat Transfer* 14, no. 1 (2023): 49-57. https://doi.org/10.37934/arnht.14.1.4957

[25] Gras-Cabrerizo, Juan R., Elena García-Garrigós, Joan R. Montserrat-Gili, Juan R. Gras-Albert, Rosa Mirapeix-Lucas, Humbert Massegur-Solench, and Miquel Quer-Agusti. "Anatomical correlation between nasal vascularisation and the design of the endonasal pedicle flaps." *Indian Journal of Otolaryngology and Head & Neck Surgery* 70 (2018): 167-173. https://doi.org/10.1007/s12070-017-1197-z

[26] Meulemans, A., F. Paycha, P. Hannoun, and M. Vulpillat. "Measurement and clinical and pharmacokinetic implications of diffusion coefficients of antibiotics in tissues." *Antimicrobial agents and chemotherapy* 33, no. 8 (1989): 1286-1290. https://doi.org/10.1128/AAC.33.8.1286

[27] Yushkevich, Paul A., Joseph Piven, Heather Cody Hazlett, Rachel Gimpel Smith, Sean Ho, James C. Gee, and Guido Gerig. "User-guided 3D active contour segmentation of anatomical structures: significantly improved efficiency and reliability." *Neuroimage* 31, no. 3 (2006): 1116-1128. https://doi.org/10.1016/j.neuroimage.2006.01.015

[28] Bullitt, Elizabeth, Donglin Zeng, Guido Gerig, Stephen Aylward, Sarang Joshi, J. Keith Smith, Weili Lin, and Matthew G. Ewend. "Vessel tortuosity and brain tumor malignancy: a blinded study1." *Academic radiology* 12, no. 10 (2005): 1232-1240. https://doi.org/10.1016/j.acra.2005.05.027

[29] Kousaka, Yasuo. Nomura, Toshiyuki. Naito, Makio. "The Possibility of the Aerosol Infection of Corona Disease COVID-19 -Analysis from the Viewpoint of Particle Technology-." *Journal of the Society of Powder Technology* 57 (2020): 526-529. https://doi.org/10.4164/sptj.57.526

[30] White, Nathan, John-David Seelig, and Sudarshan K. Loyalka. "Computation of drag and diffusion coefficient for coronavirus: I." *Journal of Aerosol Science* 157 (2021): 105806. https://doi.org/10.1016/j.jaerosci.2021.105806

[31] Nunes-Correia, Isabel, Joao Ramalho-Santos, Shlomo Nir, and Maria C. Pedroso de Lima. "Interactions of influenza virus with cultured cells: detailed kinetic modeling of binding and endocytosis." *Biochemistry* 38, no. 3 (1999): 1095-1101. https://doi.org/10.1021/bi9812524

[32] Figueroa, C. Alberto, Irene E. Vignon-Clementel, Kenneth E. Jansen, Thomas JR Hughes, and Charles A. Taylor. "A coupled momentum method for modeling blood flow in three-dimensional deformable arteries." *Computer methods in applied mechanics and engineering* 195, no. 41-43 (2006): 5685-5706. https://doi.org/10.1016/j.cma.2005.11.011

[33] Gabriel, Gülsah, Karin Klingel, Anna Otte, Swantje Thiele, Ben Hudjetz, Gökhan Arman-Kalcek, Martina Sauter et al. "Differential use of importin-α isoforms governs cell tropism and host adaptation of influenza virus." *Nature communications* 2, no. 1 (2011): 156. https://doi.org/10.1038/ncomms1158

[34] Kandeil, Ahmed, Christopher Patton, Jeremy C. Jones, Trushar Jeevan, Walter N. Harrington, Sanja Trifkovic, Jon P. Seiler et al. "Rapid evolution of A (H5N1) influenza viruses after intercontinental spread to North America." *Nature communications* 14, no. 1 (2023): 3082. https://doi.org/10.1038/s41467-023-38415-7